VIP Nanocluster Structure

DOI: 10.1002/anie.201207098

Total Structure and Electronic Properties of the Gold Nanocrystal $Au_{36}(SR)_{24}$**

*Chenjie Zeng, Huifeng Qian, Tao Li, Gao Li, Nathaniel L. Rosi, Bokwon Yoon, Robert N. Barnett, Robert L. Whetten, Uzi Landman, and Rongchao Jin**

Gold nanoparticles protected by thiolates, including thiol-terminated DNA and simple thiols,[1–5] possess extraordinary stability and constitute perhaps the most widely studied system in nanotechnology. Understanding and control of how the thiolate ligands protect the underlying gold core and of the atomic structures that the gold cores adopt with decreasing size, are issues of fundamental, and potentially practical, importance.[6] For relatively large gold nanoparticles (i.e., greater than two nanometers), electron microscopy can map out the core structure, but the surface structure (e.g. the ways that thiolates bind to gold) cannot be determined. Obtaining the total structure (i.e. the core and surface atoms) necessitates single-crystal growth of atomically precise gold nanoparticles. Recently, significant progress has been made in the chemical synthesis of ultra-small gold nanoparticles (often called nanoclusters, typically less than two nanometers) protected by thiolates, but the total structure determination of such $Au_n(SR)_m$ nanoparticles by X-ray crystallography remains a major challenge.[6,7] The reported crystal structures thus far include Au_{102}(p-MBA)$_{44}$, $Au_{25}(SCH_2CH_2Ph)_{18}$, and $Au_{38}(SCH_2CH_2Ph)_{24}$, which are all composed of non-FCC (face-centered cubic) kernels,[8–11] such as the Au_{79} decahedron in Au_{102}(p-MBA)$_{44}$,[8] the Au_{13} icosahedron in $Au_{25}(SCH_2CH_2Ph)_{18}$,[9,10] and the Au_{23} face-sharing bi-icosahedron in $Au_{38}(SCH_2CH_2Ph)_{24}$.[11] These experimental examples, as well as theoretical work,[12–14] indicate a size-dependent general trend that starts from icosahedral atomic arrangements at smaller sizes to decahedral structures at larger ones, and culminate with large clusters of FCC structure (for FCC metals).[8–19] Pertaining to the surface structures of $Au_n(SR)_m$ nanoclusters, unique "staple"-like motifs have been found, including the dimeric staple (i.e. −SR−Au−SR−Au−SR−) and the monomeric staple (i.e. −SR−Au−SR−).[8–11]

Herein, we report the discovery of an FCC-type core structure in $Au_{36}(SR)_{24}$, where SR refers to 4-*tert*-butylbenzenethiolate (denoted as SPh-*t*Bu). The emergence of FCC structure in $Au_{36}(SR)_{24}$ is surprising, given the small size of the cluster. The $Au_{36}(SR)_{24}$ particle consists of a Au_{28} kernel with a truncated FCC tetrahedron exposing (111) and (100) facets. Unlike the previously reported $Au_n(SR)_m$ nanocluster structures ($n = 25$, 38, 102),[8–11] a new type of thiolate binding mode for all-thiolate-capped nanoclusters has been discovered, that is, 12 of the 24 ligands bind to the underlying Au atoms in a simple bridging mode, with the remaining 12 thiolates forming the known dimeric staple motifs. First-principle calculations reveal a large energy gap between the highest-occupied and the lowest-unoccupied energy levels (approximately 1.7 eV), which is in agreement with the value measured by optical absorption spectroscopy. The high stability of the nanocluster originates from the geometric structure and organization of the electronic states into superatom shells. The new FCC tetrahedral Au_{28} kernel and the thiolate-bridging mode (as opposed to staple motifs) offer important implications for other possible FCC-structured gold nanocrystals, as well as for thiol binding on extended gold surfaces in self-assembled-monolayer (SAM) systems.

The synthesis of Au_{36} nanoclusters protected by SPh-*t*Bu thiolate starts with pure $Au_{38}(SCH_2CH_2Ph)_{24}$ nanoclusters. We previously reported a size-focusing method for the synthesis of $Au_{38}(SCH_2CH_2Ph)_{24}$ nanoclusters.[20] The $Au_{38}(SCH_2CH_2Ph)_{24}$ nanocluster exhibits high thermal as well as chemical stability (i.e., resistant to reduction and oxidation by common reagents).[20] Interestingly, we found that this highly stable $Au_{38}(SCH_2CH_2Ph)_{24}$ nanocluster, when reacting with HSPh-*t*Bu at 80 °C for more than 12 hours, can be transformed to a new cluster (see Supporting Information for experimental details). To determine the mass of the as-synthesized cluster, we used electrospray ionization mass spectrometry (ESI-MS). The nanocluster was found to be charge neutral; hence, CsOAc was added to the cluster solution to form a mono-Cs^+ adduct of the cluster. The positively charged adducts were then examined by ESI-MS

[*] C. Zeng, Dr. H. Qian, Dr. G. Li, Prof. R. Jin
Department of Chemistry, Carnegie Mellon University
Pittsburgh, PA 15213 (USA)
E-mail: rongchao@andrew.cmu.edu
T. Li, Prof. N. L. Rosi
Department of Chemistry, University of Pittsburgh
Pittsburgh, PA 15213 (USA)
Dr. B. Yoon, Dr. R. N. Barnett, Prof. U. Landman
School of Physics, Georgia Institute of Technology
Atlanta, GA 30332 (USA)
Prof. R. L. Whetten
School of Chemistry & Biochemistry,
Georgia Institute of Technology
Atlanta, GA 30332 (USA)

[**] R.J. thanks financial support by the Air Force Office of Scientific Research under AFOSR Award No. FA9550-11-1-9999 (FA9550-11-1-0147) and the Camille Dreyfus Teacher-Scholar Awards Program. The work of B.Y., R.N.B., and U.L. was supported by the Office of Basic Energy Sciences of the US Department of Energy under Contract No. FG05-86ER45234, and in part by the Air Force Office of Scientific Research (AFOSR). Calculations were performed at the Georgia Tech Center for Computational Materials Science. We thank Dr. Zhongrui Zhou for assistance in ESI-MS analysis.

Supporting information for this article (experimental details and electronic projected density of states) is available on the WWW under http://dx.doi.org/10.1002/anie.201207098.

(in positive mode). A clean peak at 11189.8 m/z was observed (Figure 1a). By analysis of the isotope pattern, we determined the ionized nanocluster to be mono-charged because the isotope peak spacing is unity (i.e. +1 charge state by taking

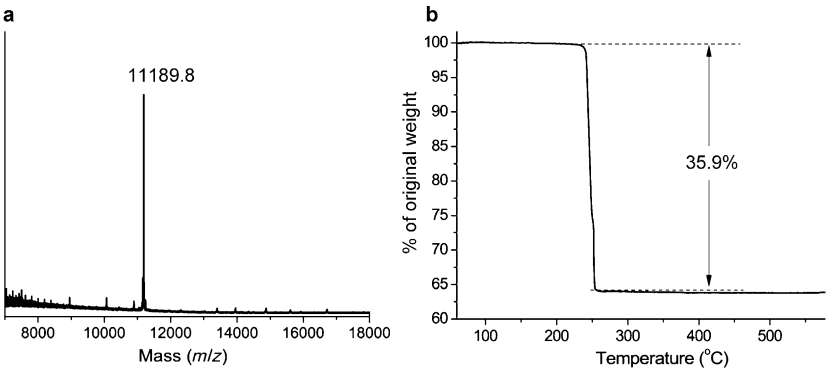

Figure 1. Characterization of $Au_{36}(SPh\text{-}tBu)_{24}$ nanoclusters. a) ESI-MS spectrum (CsOAc was added to form Cs^+-adducts with nanoclusters, b) thermogravimetric analysis (N_2 atmosphere, 10 °C min^{-1}).

the reciprocal of peak spacing); hence, the cluster mass is 11056.9 Da (after subtracting one $Cs^+ = 132.9$ Da). We next determined the Au/thiolate ratio by thermogravimetric analysis (TGA). A weight loss of 35.9% was observed (Figure 1b), which converts to a molar ratio of Au/SR = 1.5:1. By combing the cluster mass and the Au/SR ratio, the formula of the nanocluster was readily determined to be $Au_{36}(SR)_{24}$ (FW = 11057.1, deviation: 0.2 Da). It is worth noting that in previous work using a benzene-thiolate (SPh), gold clusters in this size range were identified,[21] and recently the composition of a $Au_{36}(SPh)_{23}$ cluster has been reported,[22] but in neither case could the structure be determined. It remains to be seen whether the previous $Au_{36}(SPh)_{23}$ formula[22] needs to be corrected.

Crystallization of $Au_{36}(SPh\text{-}tBu)_{24}$ was performed in CH_2Cl_2/ethanol (3:2, v/v). Rhombic single crystals were formed after two days. The crystal structure was solved by X-ray crystallography (see Supporting Information). Figure 2a shows the entire structure of $Au_{36}(SPh\text{-}tBu)_{24}$. The number of gold atoms in the metal core and the number of ligands agree perfectly with the ESI-MS determined formula. All carbon atoms were identified. No extra atoms (e.g., counterions) were found, indicating that the particle is indeed charge neutral, which is consistent with the ESI-MS and TGA results. Removal of the Ph-tBu groups revealed a D_{2d} atomic arrangement of the $Au_{36}S_{24}$ framework (Figure 2b). Four dimeric staple motifs (−SR−Au−SR−Au−SR−) can be readily identified (Figure 2c, green), evidenced by the planar geometry and the large Au_{staple}−Au_{kernel} distances (i.e., between the gold atom in the staple motif and the closest gold atom of the metal kernel, ranging from 3.019 Å to 4.072 Å, average 3.670 Å). After removing the four staple motifs, the remaining structure contained 12 sulfur atoms and 28 gold atoms (Figure 2d). At this stage, following the prevailing experience additional dimeric staples could be identified. However, careful analysis guides us to take a different course because: first, the terminal S atoms of the ostensible dimeric staple (Figure 2e, labeled **2**) form S−Au bonds that are not co-planar with the staple plane itself, thus making this protecting unit different from the standard dimeric staple one (Figure 2e, labeled **1**). Second, the Au−Au distances between a gold atom in the ostensible dimeric staple and the closest atoms of the gold kernel are rather short (ranging from 2.875 Å to 3.220 Å, average 3.061 Å), indicating quite strong bonding, which is in contrast with the large distances (approximately 3.670 Å) in the case of the standard staple motifs. Consequently, the aforementioned remaining twelve S atoms (i.e., thiolate ligands) are configured in a simple bridging bonding mode. This finding is rather surprising, as all the previously reported $Au_n(SR)_m$ structures (like Au_{102}(p-MBA)$_{44}$, $Au_{25}(SCH_2CH_2Ph)_{24}$, and $Au_{38}(SCH_2CH_2Ph)_{18}$) are exclusively protected by monomeric and/or dimeric staple motifs.

The appearance of a simple bridging mode in the $Au_{28}S_{12}$ substructure seems to

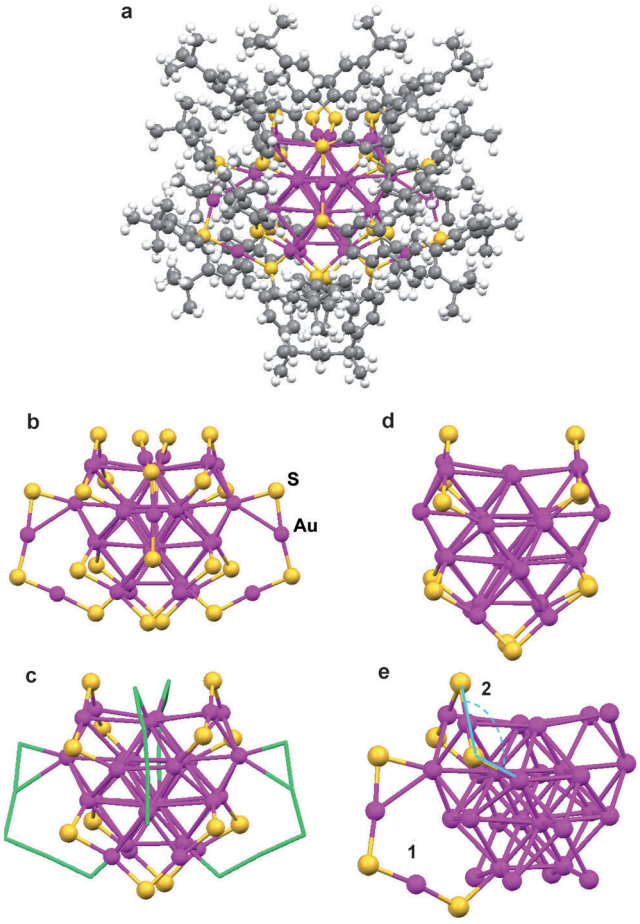

Figure 2. Total structure of $[Au_{36}(SPh\text{-}tBu)_{24}]^0$. a) The entire particle (Ph-tBu = gray atoms), b) the $Au_{36}S_{24}$ framework, c) the four dimeric staples shown in green, d) the $Au_{28}S_{12}$ framework, e) comparison of the ostensible dimeric staple (labeled **2**) and the standard dimeric staple (labeled **1**).

be closely related to the Au_{28} kernel structure. Removal of the 12 sulfur atoms reveals a layer-by-layer structure consisting of 6:8:8:6 gold atoms (Figure 3, from top to bottom), which is reminiscent of the FCC structure of bulk (or nanocrystalline)

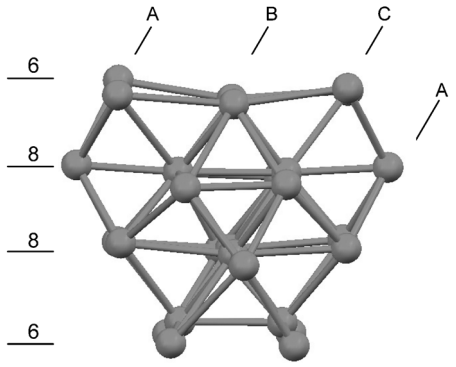

Figure 3. The Au_{28} FCC kernel structure of $[Au_{36}(SPh\text{-}tBu)_{24}]^0$.

gold. Indeed, the close-packed atomic planes register in an A:B:C:A stacking sequence (Figure 3), where A–C denote the cubic-close-packed (ccp) planes. Furthermore, the Au_{28} kernel is comprised of four interpenetrating cuboctahedra (Supporting Information, Figure S1). The cuboctahedron is a fragment of the FCC structure and can be readily constructed from it.[6] This arrangement of atoms in the 28-atom kernel is indeed the first observation of an FCC structure in $Au_n(SR)_m$ nanoclusters of discrete size. The emergence of an FCC structure of such small size is unexpected, especially in light of the icosahedral structures found in clusters of neighboring sizes, that is $Au_{25}(SR)_{18}$ and $Au_{38}(SR)_{24}$.

Alternatively, the $Au_{36}(SPh\text{-}tBu)_{24}$ cluster may be viewed as a concentric two-shell tetrahedral structure, with the first (inner) tetrahedron containing four atoms corresponding to the centers of the four cuboctahedra shown in Figure 4a. The Au_4 tetrahedron is enclosed by a second shell comprised of 24 gold atoms (Figure 4a). Overall, the morphology of the two-shell Au_{28} kernel is that of a truncated tetrahedron ($t\text{-}T_h$) (see Figure 4b). By incorporating the four dimeric staples and 12 simple bridging thiolates, the four dimeric staples span the four (111) faces along the bissecting line, while each of the six (100) faces is protected by two simple bridging thiolates (Figure 4c). In this way each of the 24 surface gold atoms of the tetrahedral $Au_4@Au_{24}$ kernel is bonded to thiolate. Only the inner Au_4 atoms are not bonded to any ligands. The average Au–Au distance in the FCC-structured Au_{28} kernel is 2.911 Å, slightly longer (approximately 1%) than the bulk Au–Au distance of 2.883 Å.[23]

As mentioned before, prior to our discovery of an FCC 28-atom gold kernel, the size-dependent structures of $Au_n(SR)_m$ nanoclusters were thought to evolve from icosahedral to decahedral and finally to FCC structures, as reflected in the structures of $Au_{25}(SCH_2CH_2Ph)_{18}$, $Au_{38}(SCH_2CH_2Ph)_{24}$, $Au_{102}(p\text{-}MBA)_{44}$, and FCC-structured $Au_{333}(SCH_2CH_2Ph)_{79}$.[8–11,16] Our work suggests a re-examination of the size-dependent structure-evolution pattern and the factors governing structural size-dependent transitions. Our results indicate that the type of thiolate ligand plays a key role in determining the structure adopted; in other words, structural stability appears to be intimately related to the identity of the thiolate ligand. Indeed, it is rather remarkable that reaction with the conjugated SPh-*t*Bu ligand drastically transforms the Au_{38} metal-core structure stabilized by the non-conjugated SCH_2CH_2Ph ligand.[11] To account for the extreme robustness of $Au_{36}(SPh\text{-}tBu)_{24}$, we suggest that one should view the ligands and the metal core as a non-divisible joint entity. The critical role of ligands is commonly overlooked. The core geometry (or structural stability) is likely to be governed, at least to some extent, by electronic effects owing to the conjugated thiolate ligands.

It might instead be argued that the ligand-induced conversion from $Au_{38}(SCH_2CH_2Ph)_{24}$ to $Au_{36}(SPh\text{-}tBu)_{24}$ might be a consequence of the "bulkiness" of the ligands, rather than having its origins in an electronic effect as discussed above. However, the observation that even very bulky thiolate ligands, such as glutathione (SG, a tripeptide with -SH), readily yield a $Au_{38}(SG)_{24}$ nanocluster, rather than a $Au_{36}(SG)_{24}$ nanocluster, serve to refute such a view. Moreover, previous work[24,25] also demonstrated that various ligands (all without the conjugation effect) give rise to $Au_{38}(SR)_{24}$ nanoclusters. Similarly, no effect of ligand bulkiness on inducing a change in cluster size was observed in the case of $Au_{25}(SR)_{18}$ either.[26] Therefore, instead of the (thermal) transformation from $Au_{38}(SCH_2CH_2Ph)_{24}$ to $Au_{36}(SPh\text{-}tBu)_{24}$ being caused by ligand bulkiness, we conclude that the conjugation effect of the SPh-*t*Bu ligand is more likely responsible for the above transformation.

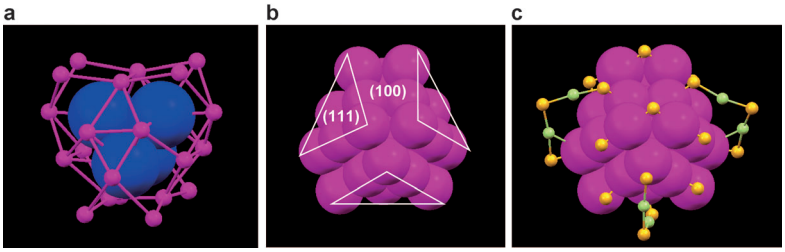

Figure 4. Tetrahedral structure of the Au_{28} kernel and surface protection by thiolate ligands. a) The inner Au_4 tetrahedron is shown in space-filled fashion, b) the two-shell Au_{28} kernel exhibits bulk-like (111) and (100) faces, c) the surface protection of the Au_{28} tetrahedron by four dimeric staples (containing 12 thiolates) and 12 bridging thiolates.

To obtain further insight into the bonding and electronic structure of the $Au_{36}(SR)_{24}$ cluster, we performed extensive first-principles calculations.[27] Figure 5 displays (in the range $-3.5\ eV \le E - E_F \le 1.5\ eV$) the projected densities of states (PDOS, see Supporting Information for details) calculated for the experimentally determined atomic coordinates (Figure 5a), for the energy-optimized structure (Figure 5b), obtained using density-functional-theory (DFT)-based relaxation of the experimental configuration), as well as for the (optimized) structure but with R = H (Figure 5c). The first outstanding feature observed is the

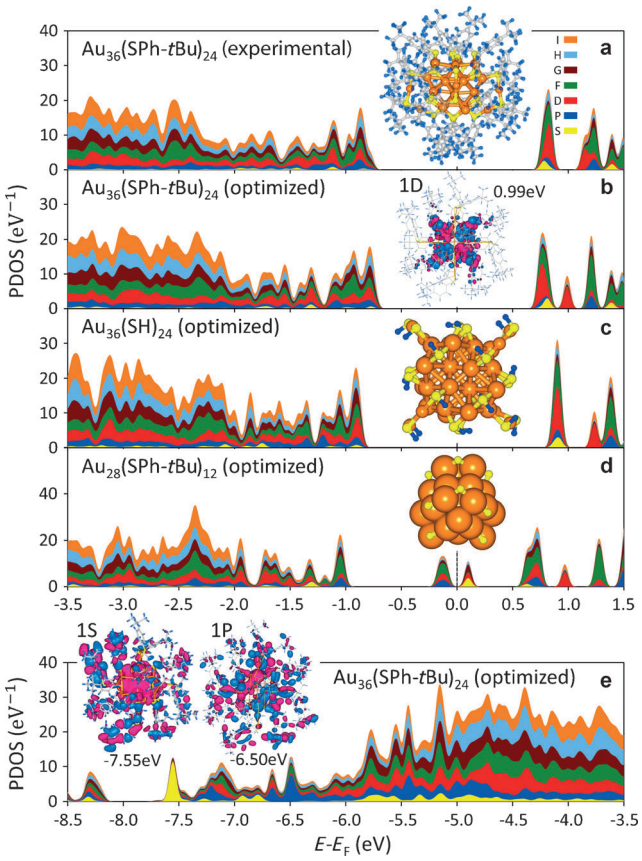

Figure 5. Electronic structure of $Au_{36}(SR)_{24}$. Projected densities of states (PDOS) for $Au_{36}(SR)_{24}$ in (a–c, e) and $Au_{28}(SR)_{12}$ in (d), with different colors corresponding to the various angular momentum contributions S, P, D, F, G, H, and I. The PDOS in (a–e) were calculated for the atomic positions of the $Au_{36}(SR)_{24}$ (and $Au_{28}(SR)_{12}$) cluster as noted. The Fermi energy E_F is the energy in the middle of the HOMO–LUMO gap. The structure of the fully protected optimized cluster is shown in the inset to (a). Au orange, S yellow, C gray, H blue. The inset in (b) is an image of one of the three unoccupied superatom 1D orbitals (different signs of the wave function are depicted in blue and pink, allowing visualization of the nodal pattern). The inset in (c) shows the optimized structure of the $Au_{36}(SH)_{24}$ cluster, and the inset in (d) depicts the 28-atom core of $Au_{28}(SR)_{12}$ with the adsorbed S atoms (the organic part was omitted for clarity), obtained from the optimized $Au_{36}(SR)_{24}$ structure by removing the four dimeric staples. The insets in (e), show the lower energy 1S and 1P orbitals calculated for the optimized cluster structure, completing the $1S^2\,|\,1P^6\,|\,1D^4$ shell.

exceptionally large HOMO–LUMO energy gap (Δ_{HL} = 1.7 eV, 1.5 eV, and 1.8 eV, respectively, in Figure 5a–c). This large gap agrees well with the optically measured one (approximately 1.7 eV), thus the optical gap represents a true HOMO–LUMO gap. This energy gap exceeds, by a large margin, those measured for other thiolate-protected gold nanoclusters in this size range, that is, 1.3 eV for $Au_{25}(SR)_{18}$ and 0.9 eV for $Au_{38}(SR)_{24}$. As previously noted, the large Δ_{HL} gap confers high stability to the cluster, endowing it with resistance to chemical attack. Inspection of the electronic structure of the cluster and the orbitals' angular momentum symmetries shows that, following an early proposal,[28] for a wide range of energies (located at the middle of the energy spectrum) the electronic wavefunctions exhibit localized character (associated with Au atomic 5d electrons), but the orbitals of states with energies near the top and bottom of the electronic spectra are of delocalized character, derived from the Au atomic 6s electrons (see representative orbital images in Figure 5b,e). The delocalized states can be assigned particular symmetries following the electronic cluster-shell-model (CSM), with a (superatom) aufbau rule: $1S^2\,|\,1P^6\,|\,1D^{10}\,|\,2S^2\,|\,1F^{14}\,|\,2P^6\,|\,1G^{18}\,|\,\ldots$ where S, P, D, F, and G correspond, respectively, to angular momenta, $l = 0, 1, 2, 3, 4\ldots$; note that the restriction of quantum number $l = 0, \ldots n-1$ in atoms is not applicable in superatoms. We note herein certain possible alterations in level ordering, as well as possible splitting of the $2l+1$ fold level degeneracy by crystal-field effects (see below). In the above CSM scheme, the vertical lines denote shell-closures (magic numbers), with each closure accompanied by the opening of a stabilizing energy gap. For the $Au_{36}(SR)_{24}$ cluster, with the number of electrons not engaged in bonding to sulfur being $36-24=12$, the aufbau rule leads to a $1S^2\,|\,1P^6\,|\,1D^4$ (superatom) configuration, which is not a closed shell. The stability of this configuration derives instead from the splitting of the fivefold degeneracy of the 1D shell owing to the non-spherical atomic arrangement in the gold cluster and the organization of the protecting ligands. Indeed, this crystal-field-like splitting is mirrored in the observation of three LUMO orbitals of 1D character in the PDOS shown in Figure 5b and its inset.

For a globular Au_{28} cluster the aforementioned aufbau rule predicts $1S^2\,|\,1P^6\,|\,1D^{10}\,|\,2S^2\,|\,1F^8$, exhibiting (4/7)-occupancy of the 1F superatom shell. Examination of the PDOS of the X-ray-determined 28-atom core leads us to conclude that the electronic structure of the tetrahedral core agrees well with the predictions of the CSM. Bonding of the twelve bridging thiolates to the cluster (see Figure 5d) leaves four electrons in the HOMO orbitals separated by a gap of close to 0.9 eV from the rest of the manifold of occupied states. The (superatom) electronic configuration of this cluster may be written as $1S^2\,|\,1P^6\,|\,1D^4$. Attachment of the four dimeric staples restores the spectrum of the completly protected $Au_{36}(SPh\text{-}tBu)_{24}$ cluster (Figure 5a,e), exhibiting the aforementioned remarkably large HOMO–LUMO gap, Δ_{HL} = 1.7 eV.

The total structure determination of the $Au_{36}(SPh\text{-}tBu)_{24}$ cluster presented herein and the theoretical insights into its bonding and electronic structure that we gained, have certain valuable implications for future investigations. First, our findings show that the structures and stability of nanoclusters are determined by a balance between maximization of the metal (gold) cohesive energy and the electronic effect of the conjugated thiolate. Along with this is our experimental (Supporting Information, Figure S2) and theoretical findings of a large (approximately 1.7 eV) HOMO–LUMO energy gap conferring to the cluster extreme stability, and originating from the (superatom) shell-structure organization of the electronic energy levels of the cluster; the occupancies of the shells and their degeneracies are both determined by the metal component of the cluster as well as by its interactions with the protecting thiolates. Second, the finding that a cluster as small as $Au_{36}(SPh\text{-}tBu)_{24}$ can have a nanocrystalline FCC core,[29] provides a strong impetus for reexamination of the

ordering and transitions between various structural motifs appearing along the size-dependent evolution of nanocluster structures.[8–11] Third, this work shows that the bridge-bonding motif of thiolates on gold particles is an important addition to the previously observed monomeric and dimeric (and the recently theoretically proposed trimeric)[30] staple motifs, as surface protectors for $Au_n(SR)_m$ nanoclusters. This finding may have implications for the still controversial case of self-assembled monolayers (SAM) on bulk gold surfaces.[7,31]

Received: September 1, 2012
Published online: November 14, 2012

Keywords: cluster compounds · face-centered cubic · gold · nanostructures · tetrahedral structures

[1] C. A. Mirkin, R. L. Letsinger, R. C. Mucic, J. J. Storhoff, *Nature* **1996**, *382*, 607.
[2] M. Brust, M. Walker, D. Bethell, D. J. Schiffrin, R. Whyman, *J. Chem. Soc. Chem. Commun.* **1994**, 801.
[3] H. Wu, H. Zhu, J. Zhuang, S. Yang, C. Liu, Y. C. Cao, *Angew. Chem.* **2008**, *120*, 3790; *Angew. Chem. Int. Ed.* **2008**, *47*, 3730.
[4] R. L. Whetten, J. T. Khoury, M. M. Alvarez, S. Murthy, I. Vezmar, Z. L. Wang, P. W. Stephens, C. L. Cleveland, W. D. Luedtke, U. Landman, *Adv. Mater.* **1996**, *8*, 428.
[5] Y. Shichibu, Y. Negishi, H. Tsunoyama, M. Kanehara, T. Teranishi, T. Tsukuda, *Small* **2007**, *3*, 835.
[6] R. Jin, Y. Zhu, H. Qian, *Chem. Eur. J.* **2011**, *17*, 6584.
[7] R. L. Whetten, R. C. Price, *Science* **2007**, *318*, 407.
[8] P. D. Jadzinsky, G. Calero, C. J. Ackerson, D. A. Bushnell, R. D. Kornberg, *Science* **2007**, *318*, 430.
[9] M. W. Heaven, A. Dass, P. S. White, K. M. Holt, R. W. Murray, *J. Am. Chem. Soc.* **2008**, *130*, 3754.
[10] M. Zhu, C. M. Aikens, F. J. Hollander, G. C. Schatz, R. Jin, *J. Am. Chem. Soc.* **2008**, *130*, 5883.
[11] H. Qian, W. T. Eckenhoff, Y. Zhu, T. Pintauer, R. Jin, *J. Am. Chem. Soc.* **2010**, *132*, 8280.
[12] C. L. Cleveland, U. Landman, T. G. Schaaff, M. N. Shafigullin, P. W. Stephens, R. L. Whetten, *Phys. Rev. Lett.* **1997**, *79*, 1873.
[13] J. Akola, M. Walter, R. L. Whetten, H. Häkkinen, H. Grönbeck, *J. Am. Chem. Soc.* **2008**, *130*, 3756.
[14] Y. Pei, Y. Gao, X. C. Zeng, *J. Am. Chem. Soc.* **2008**, *130*, 7830.
[15] G. Schmid, *Chem. Soc. Rev.* **2008**, *37*, 1909.
[16] H. Qian, Y. Zhu, R. Jin, *Proc. Natl. Acad. Sci. USA* **2012**, *109*, 696.
[17] E. G. Mednikov, M. C. Jewell, L. F. Dahl, *J. Am. Chem. Soc.* **2007**, *129*, 11619.
[18] C. Femoni, M. C. Iapalucci, G. Longoni, S. Zacchini, S. Zarra, *J. Am. Chem. Soc.* **2011**, *133*, 2406.
[19] H. Schnöckel, *Chem. Rev.* **2010**, *110*, 4125.
[20] H. Qian, Y. Zhu, R. Jin, *ACS Nano* **2009**, *3*, 3795.
[21] R. C. Price, R. L. Whetten, *J. Am. Chem. Soc.* **2005**, *127*, 13750.
[22] P. R. Nimmala, A. Dass, *J. Am. Chem. Soc.* **2011**, *133*, 9175.
[23] D. M. P. Mingos, *J. Chem. Soc. Dalton Trans.* **1996**, 561.
[24] N. K. Chaki, Y. Negishi, H. Tsunoyama, Y. Shichibu, T. Tsukuda, *J. Am. Chem. Soc.* **2008**, *130*, 8608.
[25] D. Stellwagen, A. Weber, L. G. Bovenkamp, R. Jin, H. Bitter, C. S. S. R. Kumar, *RSC Adv.* **2012**, *2*, 2276.
[26] Z. Wu, J. Suhan, R. Jin, *J. Mater. Chem.* **2009**, *19*, 622.
[27] The first-principles molecular dynamics (FPMD) method that we use has been formulated for treating neutral and charged systems, see R. N. Barnett, U. Landman, *Phys. Rev. B* **1993**, *48*, 2081. The method, which can be used for structural optimization using a conjugate-gradient-like relaxation, as well as for simulations of the dynamics of the nuclear motions evolving on the concurrently calculated Born–Oppenheimer potential energy surface, calculates the electronic structure by employing the Kohn–Sham density-functional theory (DFT) with the use of a plane wave-basis (62 Ry kinetic energy cutoff), in conjunction with soft pseudopotentials, (after N. Troullier, J. L. Martins, *Phys. Rev. B* **1991**, *43*, 19, with those for gold including scalar-relativistic corrections) and the Perdew–Burke–Ernzerhof (PBE) functional (J. P. Perdew, K. Burke, M. Ernzerhof, *Phys. Rev. Lett.* **1996**, *77*, 3865) in the generalized gradient approximation (GGA) to the exchange-correlation energy.
[28] B. Yoon, P. Koskinen, B. Huber, O. Kostko, B. von Issendorff, H. Hakkinen, M. Moseler, U. Landman, *ChemPhysChem* **2007**, *8*, 157.
[29] Recall the theoretical tetrahedral Au_{28}-core in $[Au_{44}(SR)_{28}]^{2-}$ (see D. Jiang, M. Walter, J. Akola, *J. Phys. Chem. C* **2010**, *114*, 15883) and the tetrahedral structure of the bare Au_{20} gas-phase cluster (see J. Li, X. Li, H. J. Zhai, L.-S. Wang, *Science* **2003**, *299*, 864). Additionally, see the structure determination of Au_{20} and Au_{16} (a t-T_h subunit of the 28-atom kernel described here, see Figure 3 and 4) using combined electron scattering and first-principles calculations in X. Xing, B. Yoon, J. H. Parks, U. Landman, *Phys. Rev. B* **2006**, *74*, 165423 and also Ref. [28].
[30] Y. Pei, Y. Gao, N. Shao, X. C. Zeng, *J. Am. Chem. Soc.* **2009**, *131*, 13619.
[31] P. Maksymovych, O. Voznyy, D. B. Dougherty, D. C. Sorescu, J. T. Yates, Jr., *Prog. Surf. Sci.* **2010**, *85*, 206.

